The shear behavior of the rock-concrete interface with different angles: A DEM simulation

Yingcai Hou
Department of Geotechnical Engineering, College of Civil Engineering, Tongji University, Shanghai, China

Lushan Shu
Department of Geotechnical Engineering, College of Civil Engineering, Tongji University, Shanghai, China

Kai Shen
School of Civil Engineering, Central South University, Changsha, China

Yadong Xue
Department of Geotechnical Engineering, College of Civil Engineering, Tongji University, Shanghai, China

ABSTRACT: During the whole life of a tunnel lining, the concrete-rock interface is one of the weak areas. To study the shear strength of concrete-surrounding rock interfaces, a direct shear test with a flat interface was carried out. The mechanical properties of contact surfaces with different sawtooth parameters were simulated via MatDEM based on the discrete element method. The four tooth angles (0°, 15°, 30°, and 45°) and eleven normal stresses (0.5~1.5MPa every other) were simulated. The results show that the shear strength increases with increasing normal stress for all four sawtooth angles. As the sawtooth angle increases, the shear strength increases due to the increasing cohesion and contact area. When the sawtooth angle is 15°, the failure occurs mainly along the interface. The fractures develop from the interface and the sawtooth is cut off when the angle is greater (30°and 45°) due to the mechanical occlusion.

Keywords: Concrete-rock interface, Shear behavior, Sawtooth angle, Direct shear test, MatDEM.

1 INTRODUCTION

After drilling and blasting, the surface of the surrounding rock will produce a jagged surface, as shown in Figure 1. During the whole life of a tunnel lining, the concrete-rock interface will be one of the weak areas(Wang et al., 2014).

The mechanical properties of the rock-concrete interface have a significant importance. Many researchers have studied the shear failure behaviour of the rock-concrete interface. Saiang et al. (Saiang et al., 2005) concluded that the peak shear stress at the interface was composed of the bonding force and the frictional resistance by direct shear tests on concrete-rock assemblies. In the direct shear test of concrete-rock assemblies, Tian et al.(Tian et al., 2015) found that with increasing normal stress, the bond interface showed both abrupt and progressive damage. Meng et al.(Meng et al., 2022) developed a numerical model of synthetic rock mass (SRM) based on the particle flow procedure two-dimensional (PFC2D) and carried out numerical direct shear tests to discuss the

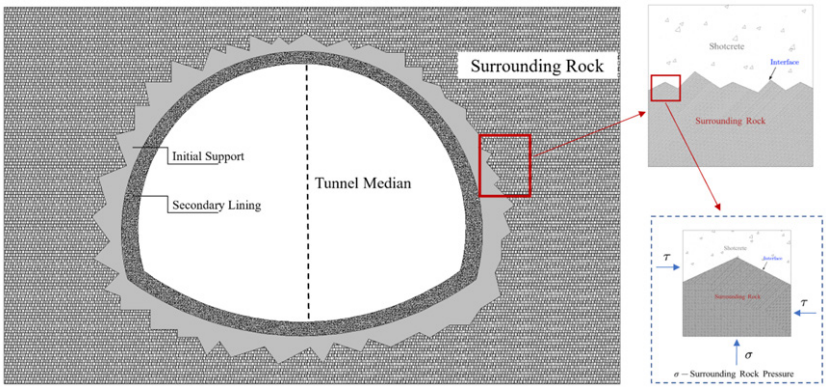

Figure 1. Schematic diagram of concrete-rock composite.

effects of joint geometry, positive stress, joint roughness and joint aperture on the shear properties of unbonded joints.

In this article, laboratory direct shear tests were first carried out. The calibration of a MatDEM model is performed based on stress-displacement curves at the normal force of 0.5 MPa. The failure process and shear strength of rock-concrete interfaces with different tooth angles were then investigated.

2 LABORATORY EXPERIMENTS AND DISCRETE ELEMENT CALIBRATIONS

2.1 The process of making a specimen

The compressive strength, tensile strength, Young's modulus and density of the rock are 30.5Mpa, 2.1Mpa, 2.8GPa and 2272 kg/m^3 respectively, while the compressive strength, Young's modulus and density of the C25 shotcrete are 26Mpa, 1.5GPa and 2280 kg/m3 respectively.

Using a cutter, the sandstone is cut to create interfaces with tooth angles of 0°. The concrete is mixed according to the specified proportions and poured into the mold box where the rock samples are placed. The concrete is compacted using a vibrating table and then the concrete-rock combination is subjected to sprinkler maintenance for 7 days, following the maintenance procedure used at the construction site. After this, any uneven parts are polished. The successful manufacture of the specimen is shown in the figure 2.

The loading system uses the CSS-1950 biaxial rheological tester from the Key Laboratory of Geotechnical and Underground Engineering, Tongji University, which is shown in figure 3. The equipment can provide a maximum pressure of 500 kN and a maximum tension of 300kN in the vertical axis and a maximum pressure of 300 kN in the horizontal axis. Loading columns can be loaded in both directions simultaneously or separately, with loading rates from 2 to 200kN/min. In this experiment, the loading range for normal forces is 0.5~1.5MPa respectively, which was divided into eleven stages of loading, with each stage spaced at 0.1 MPa. The loading rate of shear load is 0.0004 mm/s.

Figure 2. Successfully manufactured specimens.

Figure 3. Schematic of loading.

2.2 *Laboratory results and calibration results*

In this study, MatDEM, known for its high performance (Liu et al., 2017; Xue et al., 2021) was employed. Figure 4 presents the fitting of shear strength for the flat section test using the least squares method at different normal stresses. Laboratory testing yielded an internal friction angle of 55.41° and cohesion (C1) of 3.65 MPa, while numerical simulation calibrated the internal friction angle to 54.8° and cohesion (C2) to 3.65 MPa, with variances of 0.48 and 0.70, respectively (Figure 4(a)).

Comparing calibration results with laboratory experiments demonstrates good agreement, particularly at low normal stresses. The laboratory and numerical slopes of shear stress-displacement curves are 16.91 and 16.30, respectively, with peak shear strengths of 3.72 MPa and 3.75 MPa, respectively (Figure 4(b).

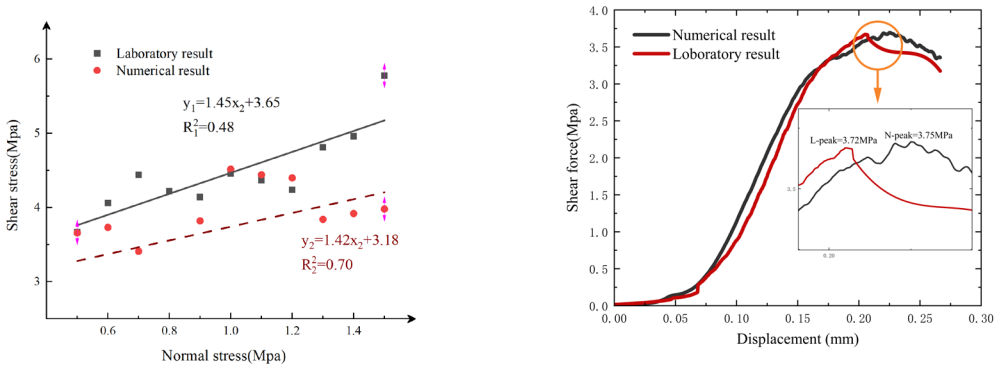

(a) Shear stress versus the normal stress (b) Shear stress versus the displacement

Figure 4. Comparison of laboratory experimental results and numerical simulation results.

3 NUMERICAL SIMULATION ARRANGEMENTS

A numerical model (Figure 5) was developed with sandstone, concrete, and an interface material. The model, measuring 100 mm × 100 mm, consisted of 63,845 randomly placed particles. It included four shear plates labeled as 1 to 4. Shearing involved applying a force to the top plate, causing leftward movement while the bottom plate remained stationary. The study examined shear deformation damage characteristics of single and multiple teeth with angles of 0°, 15°, 30°, and 45°. Peak strength and deformation were analyzed at normal stresses ranging from 0.5 MPa to 1.5 MPa. The simulation setup is detailed in Table 1.

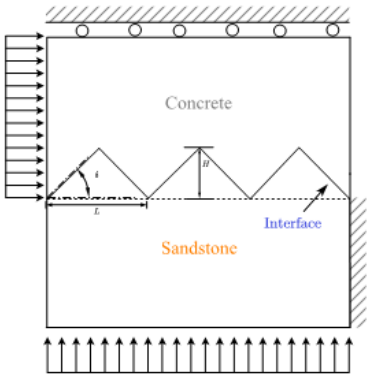

Figure 5. Diagram of the numerical simulation arrangement.

Table 1. Arrangement of Simulation.

Specimen No.	Tooth Angle/°	Normal Stress/MPa	Specimen No.	Tooth Angle/°	Normal Stress/MPa
0-1	0	0.5	30-1	30	0.5
0-2	0	0.6	30-2	30	0.6
0-3	0	0.7	30-3	30	0.7
0-4	0	0.8	30-4	30	0.8
0-5	0	0.9	30-5	30	0.9
0-6	0	1.0	30-6	30	1.0
0-7	0	1.1	30-7	30	1.1
0-8	0	1.2	30-8	30	1.2
0-9	0	1.3	30-9	30	1.3
0-10	0	1.4	30-10	30	1.4
0-11	0	1.5	30-11	30	1.5
15-1	15	0.5	45-1	45	0.5
15-2	15	0.6	45-2	45	0.6
15-3	15	0.7	45-3	45	0.7
15-4	15	0.8	45-4	45	0.8
15-5	15	0.9	45-5	45	0.9
15-6	15	1.0	45-6	45	1.0
15-7	15	1.1	45-7	45	1.1
15-8	15	1.2	45-8	45	1.2
15-9	15	1.3	45-9	45	1.3
15-10	15	1.4	45-10	45	1.4
15-11	15	1.5	45-11	45	1.5

4 NUMERICAL SIMULATION RESULTS AND ANALYSIS

4.1 Shear strength in different sawtooth angles

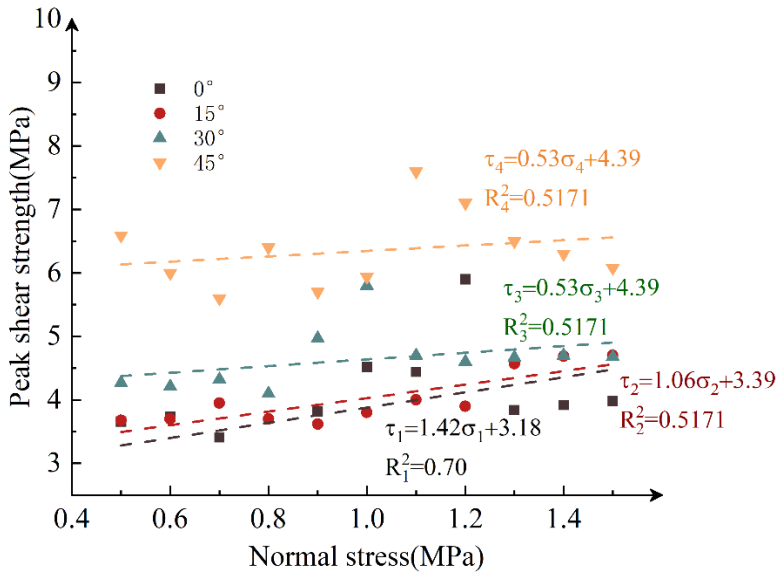

Figure 6. Peak shear strength of different angular tooth angles under different normal forces.

Figure 6 shows peak shear strength variation with tooth angle for the rock-concrete interface under different vertical forces. Shear strength increases with greater angle due to improved mechanical occlusion. At 15°, strength rises marginally, but at 30°, it rises significantly. A sharp increase occurs at 45°, revealing a stronger effect beyond a critical angle. Additionally, increased contact area with greater tooth angle enhances cohesion (y-axis intercept).

As the normal stress increases, the peak shear strength increases for all four tooth angles, which is consistent with the Mohr—Coulomb law. However, the increasing rate is different for different saw angle. The higher sawtooth angle, the lower increasing rate. It shows that the mechanical occlusion accounts for more shear resistance when the sawtooth angle is greater. The rise of cohesion force caused by the increasing vertical force takes a much smaller percentage.

4.2 Failure process of the rock-concrete interface

Figure 7 illustrates the failure process of the rock-concrete interface with different sawtooth angles. Initially, during the loading stage, the lower part (sandstone) undergoes lateral expansion under vertical force (Figure 1(a), (d), (g), and (j)). The flat interface primarily experiences damage without additional cracks, leading to direct sliding characteristics. At a 15° sawtooth angle, cracks propagate along the interface, and significant fractures appear on the sawtooth's back slope. However, the sawtooth gets truncated at a 30° angle, with some fractures originating from the interface due to mechanical occlusion providing shear resistance. At a 45° angle, the effect of mechanical occlusion intensifies, resulting in more fractures and cracks. These findings highlight that mechanical occlusion strengthens shear resistance as the sawtooth angle increases. Beyond a certain value (30° and 45°), the sawtooth breaks. It is worth noting that contact area and adhesive force also increase with the sawtooth angle, contributing to the additional force required for sawtooth formation through mechanical occlusion. In conclusion, larger sawtooth angles play a crucial role in enhancing the maximum tolerable shear force of the rock-concrete interface.

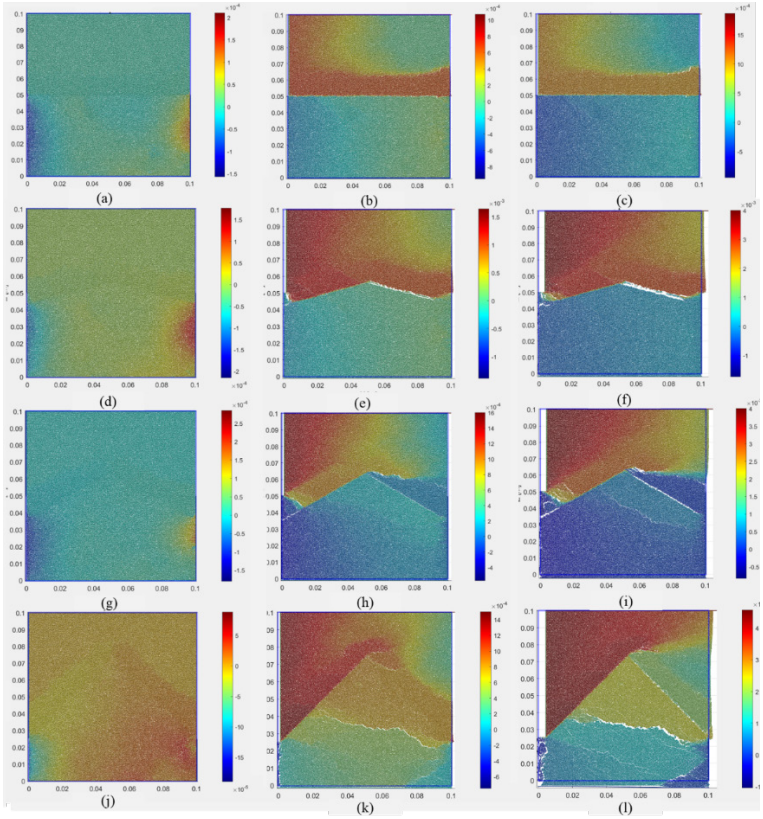

Figure 7. The failure process of the rock-concrete interface with different sawtooth angles with concrete on the top of sandstone.

5 CONCLUSION

Through laboratory direct shear tests and DEM numerical simulation, main conclusions are listed as follows.

1. A laboratory shear test was conducted. The shear behavior can be well simulated by the MatDEM software. Test results were used to the DEM calibration for further numerical simulations.
2. The shear strength increases for all four sawtooth angles with increasing normal stress. As the sawtooth angle increases, the shear strength increases due to the increasing cohesion and contact area.
3. When the sawtooth angle is 15°, the failure occurs mainly along the interface. The fractures develop from the interface and the sawtooth is cut off when the angle is greater (30°and 45°) due to the mechanical occlusion.

ACKNOWLEDGEMENTS

The authors wish to thank the support from the China Atomic Energy Authority(CAEA) for China's URL Development Program and the Geological Disposal Program. National Key R&D Program of China(2021YFB2600800).

REFERENCES

Liu, C., Xu, Q., Shi, B., Deng, S., & Zhu, H. (2017). Mechanical properties and energy conversion of 3D close-packed lattice model for brittle rocks. *Computers & Geosciences*, *103*, 12–20. https://doi.org/10.1016/j.cageo.2017.03.003

Meng, F., Song, J., Wang, X., Yue, Z., Zhou, X., & Wang, Z. (2022). Mechanical behavior of non-persistent joints with different geometric configurations and roughness in solid rock and concrete material. *Construction and Building Materials*, *337*, 127564. https://doi.org/10.1016/j.conbuildmat.2022.127564

Saiang, D., Malmgren, L., & Nordlund, E. (2005). Laboratory tests on shotcrete-rock joints in direct shear, tension and compression. *Rock Mechanics and Rock Engineering*, *38*(4), 275–297. https://doi.org/10.1007/s00603-005-0055-6

Tian, H. M., Chen, W. Z., Yang, D. S., & Yang, J. P. (2015). Experimental and Numerical Analysis of the Shear Behaviour of Cemented Concrete-Rock Joints. *Rock Mechanics and Rock Engineering*, *48*(1), 213–222. https://doi.org/10.1007/s00603-014-0560-6

Wang, S. Y., Sloan, S. W., Sheng, D. C., Yang, S. Q., & Tang, C. A. (2014). Numerical study of failure behaviour of pre-cracked rock specimens under conventional triaxial compression. *International Journal of Solids and Structures*, *51*(5), 1132–1148. https://doi.org/10.1016/j.ijsolstr.2013.12.012

Xue, Y., Zhou, J., Liu, C., Shadabfar, M., & Zhang, J. (2021). Rock fragmentation induced by a TBM disc-cutter considering the effects of joints: A numerical simulation by DEM. *Computers and Geotechnics*, *136*, 104230. https://doi.org/10.1016/j.compgeo.2021.104230